# Strength and variability of the Oligocene Southern Ocean surface temperature gradient

**Frida Hoem** ( f.s.hoem@uu.nl )
Utrecht University https://orcid.org/0000-0002-8834-6799
**Isabel Sauermilch**
Utrecht University
**Adam Aleksinski**
Purdue University
**Matthew Huber**
Purdue University
**Francien Peterse**
Utrecht University https://orcid.org/0000-0001-8781-2826
**Francesca Sangiorgi**
Utrecht University
**Peter Bijl**
Utrecht University

**Article**

**Keywords:**

**Posted Date:** April 15th, 2022

**DOI:** https://doi.org/10.21203/rs.3.rs-1516446/v1

# Strength and variability of the Oligocene Southern Ocean surface temperature gradient

**F. S. Hoem[1], I. Sauermilch[1], A.K Aleksinski[2], M. Huber[2], F. Peterse[1], F. Sangiorgi[1] and P. K. Bijl[1]**

*[1]Department of Earth Sciences, Utrecht University, Utrecht, The Netherlands.*

*[2]Department of Earth, Atmospheric and Planetary Sciences, Purdue University, West Lafayette, USA.*

**ABSTRACT**

Large Oligocene Antarctic ice sheets co-existed with warm adjacent ocean waters. To provide a broad Southern Ocean perspective to such warmth, we reconstruct the strength and variability of the Oligocene Australian-Antarctic latitudinal sea surface temperature (SST) gradient. Our Oligocene $TEX_{86}$-based SST record from offshore southern Australia shows temperate (20–29°C) conditions throughout, despite northward tectonic drift. A persistent SST gradient (~5–10°C) exists between Australia and Antarctica, which becomes larger during glacial maxima. The SST gradient increases from ~26 Ma onwards, due to decreasing Antarctic-proximal SSTs. Meanwhile, benthic foraminiferal oxygen isotope decline indicates ice loss/deep-sea warming. These contrasting patterns are difficult to explain by greenhouse gas forcing alone. Timing of the SST cooling coincides with deepening of Drake Passage and fits well with results of ocean model experiments, suggesting Antarctic-proximal cooling. We conclude that Drake Passage deepening cooled Antarctic coastlines which enhanced thermal isolation of the Antarctic ice sheet.

## INTRODUCTION

Southern high-latitude sea surface temperature (SST) records from the Oligocene (33.9–23.0 Ma)[1-4] show unexpectedly warm-temperate conditions, despite evidence for the coeval presence of large Antarctic ice sheet[5], which extended to the margins of the continent[6,7]. This apparent contradiction requires reconciliation[8]. A warm Oligocene Southern Ocean could be the result of generally high atmospheric $pCO_2$ concentrations (300–700 ppm; https://www.paleo-co2.org[9]), but higher $pCO_2$ would also be associated with reduced ice volume[10]. Furthermore, since enhanced Antarctic ice volume should have cooled marginal seas[11] the mystery of warm high latitude SSTs and greater ice volume grows. One alternative hypothesis is that marine ice sheet terminations were restricted to the southernmost parts of the Antarctic margin, facilitated by a higher-than-modern Antarctic paleotopography[12], while elsewhere the ice sheets were mostly terrestrial (e.g., refs. [13,14]), limiting the Antarctic glacial cooling effect on proximal SSTs[15]. Or as a final hypothesis, a restricted width of critical Southern Ocean gateways (Tasmanian Gateway and Drake Passage) may have played a role in ocean heat redistribution[16]. Closed ocean gateways, which can reduce meridional temperature gradients by enhancing ocean poleward heat transport or by increasing local radiative heating through albedo feedbacks or enhanced atmospheric moisture transport[17,18] may thereby have sustained warm SSTs while simultaneously maintaining terrestrial ice sheets. Each of these factors (radiative forcing, ice sheet configuration and tectonic changes) would have had a unique spatial fingerprint of Southern Ocean SST changes relative to those at the Antarctic continental margin and unravelling the complexities is challenging. Atmospheric $pCO_2$ associated radiative forcing would be expected to cause globally synchronous temperature trends on both long- and orbital-time scales, although with a degree of polar amplification. Ice sheet growth increase poleward heat transport[19], but at the same time

induces local cooling at the Antarctic margin[11]. The different response to Antarctic glaciation in different model experiments (Supplementary Table 1) can be attributed to subtle changes in paleogeography and model set-up[20]. In any case, ice volume change has the most effect close to the Antarctic continent, and is further evident in benthic foraminiferal $\delta^{18}O$ [21] and deep-sea cooling[22]. Finally, opening of gateways would result in profound cooling of Antarctic proximal waters [23,24] while leaving the rest of the world's sea water temperatures largely unaffected[11,17]. Thus, as opposed to ice volume changes, gateway opening cause a stepwise, unidirectional change in temperature: changes in SSTs could then be stratigraphically linked to phases of gateway opening[24,25]. Currently, Oligocene SST records from the subtropics are lacking, which hinders establishing the latitudinal SST gradients needed to provide context for ice-proximal SST changes, and to evaluate the possible factors that drove the evolution of Oligocene Southern Ocean surface conditions.

Here, we present $TEX_{86}$ based SST estimates from Late Eocene–Early Miocene ODP Site 1168 sediments (339–765 mbsf), west of Tasmania (red dot in Figure 1). To explore the evolution of the Oligocene SST gradient across the Tasmanian Gateway region, we compared our data with $TEX_{86}$ based SSTs from east of Tasmania (ODP Site 1172)[26], west of the Campbell Plateau (DSDP Site 277)[4], north of the Ross Sea (DSDP Site 274)[2], offshore Wilkes Land (IODP Site U1356 [1] and DSDP Site 269 [27]) and inorganic chemical weathering indices recording terrestrial temperature from the Cape Roberts Project (CRP) in the Ross Sea[28] (Figure 1). These SST records are compared to the temperature distribution in a coarse-resolution (3° horizontal), fully coupled general circulation model (GCM) following Kennedy-Asser, et al., [23]; HadCM3L – Hadley Centre Coupled Model), which simulates equilibrium temperature response to $CO_2$

forcing, and the role of ice volume and geographic boundary conditions of the Early- and Late Oligocene (33.9–28.1, 28.1–23 Ma). Details of ocean heat transport and consequences of local bathymetry are subsequently investigated comparing SST results to high horizontal resolution (0.25°) ocean-only model simulations[24]. Our results show an increase in the SST gradient across the Southern Ocean starting at 26 Ma, when Antarctic-proximal SSTs cooled. This is in contrast to a synchronous decrease in global benthic foraminiferal $\delta^{18}O$ indicating ice mass loss/deep sea warming. Considering the potential drivers of such cooling, we conclude that the Late Oligocene Antarctic-proximal SST cooling is not primarily driven by changes in $pCO_2$ and ice sheet configuration, but by paleogeographic configurations.

## RESULTS

Our SST record is based on 123 samples from ODP Site 1168 which were processed for $TEX_{86}$ paleothermometry. Twenty-one showed potential for non-thermal overprints, thereby considered unreliable, and discarded from the dataset (see Supplementary information). Results indicate Late Eocene–Early Miocene (35–20 Ma; red line Figure 2b; Supplementary Table 2) SSTs of 20–29°C (± 4°C standard error). The amplitude of SST variability was high (5–7°C) around 28 Ma and from 25 Ma onwards, and low (~3°C) between 32–29 Ma and 27–25 Ma. Our record indicates 4°C cooling (from 27 to 23°C) across the Eocene–Oligocene transition (ca. 34 Ma) and then a return to high temperatures, ~29°C, at 33.2 Ma. Temperatures then gradually cooled until ~28 Ma. A transient warming of 6°C occurred from 27.8–24.3 Ma, followed by a gradual cooling from 24.3–22.2 Ma. The $TEX_{86}$-based SSTs are generally warm and in line with $U^{k'}_{37}$-based SSTs of 19°C to 29°C derived from the same records for the 29.8–16.7 Ma interval[29] (Supplementary Figure 7). The $U^{k'}_{37}$-based SST record shows a more prominent Late Oligocene

91 warming, although $U^{k'}_{37}$-based SSTs remains within the variability of the $TEX_{86}$-based SST
92 record. Further support for the warm-temperate SSTs comes from dinoflagellate cyst (dinocyst)
93 assemblages analyzed on the same samples, which suggest stable, open marine and warm-
94 temperate conditions[30].
95
96 **DISCUSSION**
97 **Temperature gradient across the Australian-Antarctic Gulf**
98 We focus the discussion on the SST gradient across the Australian-Antarctic Gulf (AAG),
99 between Sites 1168 and U1356 in the proxy data compilation (arrows, Figure 2), due to their
100 high temporal resolution, while Sites 1172, 277, 274 and 269 will offer a broader regional
101 context. We note a persistent SST gradient (5–10°C) between the Antarctic-proximal (Site
102 U1356) and the subtropical (Site 1168) sites, albeit smaller than at present-day (~14°C)[31]. Still,
103 this implies that (polar) frontal systems separated water masses latitudinally already in the
104 Oligocene AAG. The Early Oligocene latitudinal separation of water masses is further
105 corroborated by the strong latitudinal separation in dinocyst assemblages from ~30 Ma onwards
106 between the Australian (Site 1172[3] and 1168[30], relatively oligotrophic) and Antarctic (Site
107 U1356[13], 269[27] and 274[2], eutrophic, upwelling) margins of the AAG.
108 The reconstructed SST gradient is in line with the output of two Oligocene GCM simulations
109 (Figure 3), albeit absolute SSTs are in general lower throughout the region in the model
110 simulations (10–20°C; Figure 2, Figure 3F) than in the $TEX_{86}$-based SST records (15–29°C).
111 This could be the result of a warm bias in the $TEX_{86}$ proxy (e.g., Hartman, et al. [1]), as suggested
112 by the slightly cooler $U^{k'}_{37}$-based SSTs[29] (Supplementary Figure 7) and/or to too low climate
113 sensitivity in the GCMs. The two different ice sheet sizes in the Early- and Late Oligocene

simulations can be used to evaluate the effects of the glacial-interglacial variability in ice sheet size as well as the effect of long-term changes in geographic boundary conditions on the simulated latitudinal SST gradient. Interestingly, while the Site U1356 proxy data do show strong SST variability over glacial-interglacial cycles, two different ice sheet sizes in the Early- and Late Oligocene GCM simulations is of little (~1°C) impact to the simulated latitudinal SST gradient (Figure 3B). We also note that the difference in amplitude of glacial-interglacial SST change between offshore Australia and Antarctica is too large to be caused only by greenhouse gas induced radiative forcing with a factor of polar amplification. Therefore, we ascribe the high amplitude temperature signal to migrating ocean frontal systems. The small effect of the northward tectonic drift of Site 1168 on regional SSTs, indicates that the subtropical front (STF) likely migrated northward along with the Australian landmass, as has been suggested from microfossil data[30]. This effect is further muted at Site 1168, because Australia is hindering northward migration of the STF, which explains the smaller temperature swings offshore Australia on orbital timescales.

**Late Oligocene paleogeographic, ocean temperature, atmospheric $pCO_2$ and ice volume changes.**

In the Late Oligocene we note the substantially increasing temperature gradient across the AAG latitudinal transect from 6°C prior to 26 Ma to >10°C by 23 Ma (Figure 2). This is mostly due to unidirectional progressive cooling of the Antarctic-proximal SST record at Site U1356 and stepwise air temperature cooling at CRP[28] starting at around 26 Ma, opposite to stable SSTs at Site 1168 and the benthic foraminiferal $\delta^{18}O$ record showing Late Oligocene warming and ice mass loss. The Antarctic-proximal cooling continues into the Miocene, where the $\delta^{18}O$ record

also show deep ocean cooling. Meanwhile the subtropical SSTs at Site 1168 show a Late Oligocene warming coincident with trends in $\delta^{18}O$ record (Figure 2D). The slightly cooler Late Oligocene SSTs at Site 269, northeast of Site U1356, have been attributed to its proximal location to upwelling[27], while the cooler SSTs at Site 274 is attributed to its higher latitude and proximity to the colder Ross Sea[2], as also inferred from the air temperature record at CRP[28] (Figure 2C). We break down the complex interplay of forcings and feedbacks that kept the Early Oligocene Southern Ocean warm and caused cooling of the Wilkes Land Antarctic Margin at 26 Ma – changes in atmospheric $pCO_2$ levels, ice volume or paleogeography (Table 1). Indeed, Late Oligocene atmospheric $pCO_2$ does gradually decline (700–300 ppm[9]; Figure 2E)**.** However, the contrasting paleotemperature trends, with Antarctic-proximal SSTs cooling, subtropics remaining warm and equatorial areas warming, question the role of $pCO_2$ as primary driver of Late Oligocene Southern Ocean temperature trends. In community earth system model simulations by Goldner, et al. [11], the expansion of Antarctic ice sheets generates cooling of 6°C at the Antarctic margin, while in atmosphere - ocean GCM model simulations by Knorr and Lohmann[19] an expanded ice sheet would cause regional warming at the Antarctic margin (Supplementary Table 1). Nonetheless, an expanding Late Oligocene ice volume is unlikely given the decreasing benthic $\delta^{18}O$ indicating loss of Antarctic ice volume with deep-sea warming[21,22], which has been ascribed to local tectonism on Antarctica[12,15]. Moreover, the Early- and Late Oligocene GCM model results showed little effect of ice volume changes on the Southern Ocean SST gradient (Figure 3B). The Late Oligocene breakdown of the relationship between SST, deep ocean temperature, atmospheric $pCO_2$ and ice volume [8]suggests that Antarctic proximal SST cooling was not limited to $pCO_2$ changes or glaciation-induced negative feedback[11], but probably also affected by paleogeographic configurations.

**Tectonic deepening of Drake Passage caused cooling along Antarctic Margin**

Conventional climate models had suggested that opening of Southern Ocean gateways had little effect on poleward ocean heat transport and polar climate[11,32]. However, recently, the importance of high-resolution ocean model simulations in such experiments has been underlined[17,20]. Eddy-permitting model simulations[24] show that deepening of the second of two Southern Ocean gateways (Drake Passage and Tasmanian Gateway) below 300 m drives surface water cooling at the Antarctic margin (up to 5°C), while leaving the rest of the Southern Ocean with little relative temperature changes (Figure 3C). At 26 Ma, this is exactly what can be seen in the SST compilation: The SST at the STF remains relatively stable despite northward migration and the Antarctic proximal Site U1356 show profound cooling (Figure 2), while the benthic $\delta^{18}O$ records shows apparent global warming/ice loss. The gradual northward migration of Australia could have progressively invited a larger volume of east flowing STF water to follow the southward route around Australia[16], without changing the absolute temperature in the STF region. This southward route would also progressively line up better with the westerly wind belt, strengthening the proto-Antarctic Circumpolar Current[33,34]. A strengthened proto-Antarctic Circumpolar Current would deflect the warm poleward extension of the subpolar gyres, including the proto-Leeuwin Current away from Antarctica, and reduce heat transport towards Wilkes Land Antarctic Margin, increasing polar isolation[24]. Crucially, the timing of this observed gradient increase coincides with evidence from kinematic reconstructions of Drake Passage[25] showing a first deep ocean connection around 26 Ma. Also, sediments from the South Pacific indicate the formation of the proto-Antarctic Circumpolar Current in the Late Oligocene (ca. 25–23 Ma)[35]. Thus, we deduce that despite proximity to the Tasmanian Gateway, the deep opening of Drake Passage in the Late Oligocene induced strong increase in the Southern Ocean

SST gradient and cooling of Antarctic surface waters, also in the Tasmanian Gateway area. Although radiative forcing ($CO_2$, orbital variations) is (likely) the primary driver of the Cenozoic climatic evolution (e.g. Cramwinckel, et al. [36]; Hutchinson, et al. [37]), we here demonstrate the fundamental role paleogeography plays on Southern Ocean and Antarctic climate.

## CONCLUSION

Our $TEX_{86}$-based SST record from the Oligocene Tasmanian Margin (ODP Site 1168), representing the SST evolution of the STF, in comparison with the benthic foraminiferal $\delta^{18}O$ compilation, $pCO_2$ estimates, regional SST records, and model simulations, show the following:

- The latitudinal SST gradient across the widening AAG was ~6–8 °C in the Late Eocene–Early Oligocene, and increasing from 26 Ma, when Antarctic proximal cooling started.
- The latitudinal SST gradient is larger during glacial than interglacial intervals. This is a result of latitudinal migrations of ocean frontal systems, which are limited at the northern boundary of the Southern Ocean by the position of Australia.
- Long term trends in Antarctic ice volume and polar amplification due to decreasing $pCO_2$ cannot alone explain the Antarctic proximal cooling starting at 26 Ma. We correlate this cooling to the first deep opening of Drake Passage, which decreased the strength of subpolar ocean gyres and southward heat transport, enhancing Antarctic thermal isolation and circumpolar flow.

## METODS

### Site description, depositional setting and age model

We reconstruct the changes in sea surface temperature from the subtropical front region by studying marine sediments (766–339 mbsf) from Ocean Drilling Program (ODP) Site 1168 (42°38′40″ S, 144°25′30″ E, present water depth: 2463 m). The site is situated 70 km off the west Tasmanian coast, north of the oceanographic subtropical front, where relatively carbon rich siliciclastic sediments have filled the graben basin between two basement highs (~ 25 km length) since the Late Eocene until Early Oligocene and continental slope sedimentation of calcium carbonate rich sediments thereafter[30,38]. A detailed description of the site location, depositional setting and oceanographic setting has been given in Hoem, et al. [30]. For the age model, we updated ages of tie points interpolated (cf. Stickley, et al. [39]; updated to GTS2012 ages[40] in Hoem, et al. [30]) with the exemption of one last occurrence datum of foraminifera *Subbotina angiporoides*. We interpolated a loess smooth (span of 0.1) through age tie points to obtain the ages of our samples (Supplementary Figure 1).

**$TEX_{86}$ paleothermometry**

In order to reconstruct sea surface temperature (SST), we applied the $TEX_{86}$ (TetraEther indeX of 86 carbon atoms) proxy[41], which is based on the temperature-dependent cyclisation of isoprenoidal glycerol dialkyl glycerol tetraethers (GDGTs) produced by thaumarchaeotal membrane lipids. A total of 123 samples spanning the period between 35 and 20 Ma (766–339 mbsf) were processed for analysis of GDGTs (Supplementary Methods; Supplementary Table 2). GDGTs were extracted from powdered and freeze-dried sediments using a Milestone Ethos X microwave or accelerated solvent extractor system. Lipid extracts were separated into an apolar, ketone and polar fraction by Silica gel column chromatography. GDGT standard was added to the polar fraction and filtered over a 0.45 μm polytetrafluoroethylene filter. The dissolved polar

fractions were injected and analysed by high-performance liquid chromatography–mass spectrometry (HPLC–MS) at Utrecht University, using double-column separation[42]. GDGT peaks in the HPLC chromatograms were integrated using ChemStation software. A more detailed description can be found in the Supplementary Methods.

$TEX_{86}$ was calculated as defined by Schouten, et al. [41]:

$$`TEX_{86}` = \frac{GDGT-2+GDGT-3+Cren'}{GDGT-1+GDGT-2+GDGT-3+Cren'} \quad (1)$$

$TEX_{86}$ results were examined for non-thermal overprints (described in detail in Supplementary Methods) to verify the reliability of their SST signal (Supplementary Table 2; Supplementary Figure 2-6) and compared to an alkenone-derived ($U^{k'}_{37}$) SST record from the same site[29] (Supplementary Figure 7). For systematic calculation of GDGT ratios, data analysis, visualization, and evaluation of isoGDGT, brGDGT and/or brGMGT data, we utilized the R script of Bijl, et al. [26]: https://github.com/bijlpeter83/RGDGT.git. We uploaded the measured peak areas (Supplementary Table 2) of GDGTs in the R script and calculated and plotted fractional abundances, overprinting indices and paleotemperature time series (Supplementary Figures 2-4).

In order to translate the $TEX_{86}$ values into SSTs, we used the regionally varying, Bayesian calibration; BAYSPAR SST (prior mean of 30°C, prior standard deviation of 20) of Tierney and Tingley [43] (Supplementary Figure 5). The BAYSPAR method compares measured $TEX_{86}$ values with similar values in the modern SST observations, obtained from surface sediment samples, to derive linear regression parameters: BAYSPAR propagates uncertainties in the surface sediment data into resulting temperature predictions[43]. SST estimates obtained with the exponential

transfer function BAYSPAR are very similar to the $TEX_{86}$-based SSTs produced by the exponential function from Kim, et al. [44] and linear function by O'Brien, et al. [45](Supplementary Figure 6), varying, at most, by 2°C.

## Temperature data compilation

We compiled existing Oligocene $TEX_{86}$ data and applied the BAYSPAR SST calibration [43] for consistency, from east of Tasmania: ODP Site 1172[26], north of the Ross Sea: DSDP Site 274[2], offshore Wilkes Land: IODP Site U1356[1] and DSDP Site 269[27]. The age model for the terrestrial temperature records from the Ross Sea: Cape Roberts Project (CRP)[28] based on Lavelle [46], McIntosh [47], and Florindo, et al. [48], was converted to GTS2012 ages[40] for the purpose of this paper.

## Fully coupled climate model

For model-data intercomparisons, we utilized a suite of general circulation model (GCM) HadCM3BL-M2.1aE model experiments, with full atmospheric coupling, compiled by the Bridge Consortium of the University of Bristol (found at http://www.bridge.bris.ac.uk/resources/simulations, Kennedy-Asser, et al. [23]). Simulations that were selected for comparison (Figure 3b) were built using boundary conditions, developed by Getech Group plc, appropriate for Rupelian and Chattian-age paleogeographies with either a closed or open Drake Passage, using varying ice sheet constructions (either no ice sheet, East Antarctic Ice Sheet only, or full Antarctic Ice Sheet), and varying $pCO_2$ concentrations (either 560 or 1120 ppm) (Supplementary Table 3).

## High resolution eddy resolving ocean model

The presented high-resolution ocean simulations (Figure 3C) are taken from Sauermilch, et al. [24]. It uses the Massachusetts Institute of Technology ocean general circulation model (MITgcm)[49] with a circum-Antarctic model domain (from 84°S to 25°S). The spatial resolution is 0.25° (3-25 km resolution) and vertical resolution contains 50 layers (ranging from 10 m at the sea surface to 368 m at the sea floor). Southern Ocean paleogeography is reconstructed to the Late Eocene (38 Ma) position using the plate tectonic model of Matthews, et al. [50]) in a paleomagnetic reference frame [51].

The model is ocean-only and atmospheric forcing are taken from a coupled atmosphere-ocean simulation (GFDL CM2.1) run with atmospheric $pCO_2$ concentration of 800 ppm[52]. A restoring time scale of 10 days is applied. Although not directly coupled to the atmosphere or ice sheet, the resolution of the ocean model is higher than most previous paleo-simulations and permits the formation of ocean eddies which are responsible for the majority of the ocean heat transport[53]. The high-resolution model is less diffusive, allowing accurate simulation of subsurface velocities and current structure. In addition, detailed paleobathymetry features such as the seafloor roughness, but also small depth changes in the critical gateway regions, Tasman Gateway and Drake Passage, can be accurately resolved. To accommodate this advantage, new high-resolution paleobathymetry grids are used[54] which are able to reconstruct detailed seafloor roughness features, such as seamounts and fracture zones, that have a substantial impact on the large-scale ocean circulation (e.g. LaCesca, et al. [55]). See Sauermilch, et al. [24] for further details about the methodology of the high-resolution ocean model and paleobathymetry reconstruction.

## DATA AVAILIABILITY

The GDGT results from ODP Site 1168 (Supplementary Table 2) is uploaded to the Zenodo repository: DOIXX(provided when the paper is accepted).

## TABLE AND FIGURES

**Table 1. Scenarios to explain Late Oligocene trends in SST and deep sea $\delta^{18}O$**

| Scenario | Antarctic proximal SST | Subtropical SST | Deep ocean $\delta^{18}O$ | Evaluation |
|---|---|---|---|---|
| Late Oligocene proxy data | Cooling | Stable | Decreasing | Target |
| 1. $pCO_2$ decrease | Cooling | Cooling | Increasing | Failure |
| 2. Antarctic Ice Sheet expansion | Cooling | Stable/slight cooling | Increasing | Failure |
| 3. Deepening of oceanic gateways and Antarctic ice loss | Cooling | Stable | Decreasing | Success |

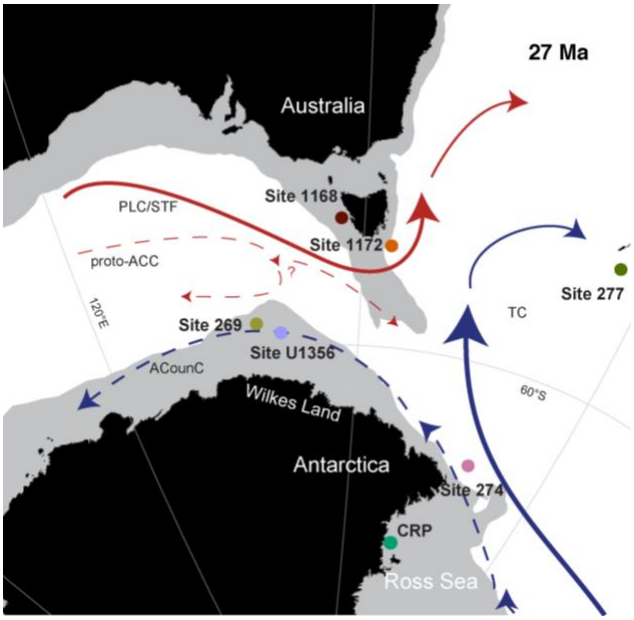


**Figure 1. Paleogeographic map of the Oligocene locations of study sites and prevailing ocean currents:**

The approximate paleogeography at 27 Ma is reconstructed through G-plates (http://www.gplates.org), based on the global geodynamic rotation model from Müller, et al. [56]. Black represents the outline of modern coastlines. The grey outline corresponds to the modern 2000 m water depth contour. PLC=Proto-Leeuwin Current, STF=Subtropical front, TC=Tasman Current, proto-ACC=proto-Antarctic Circumpolar Current and ACountC=Antarctic counter current (after Houben, et al. [3]).

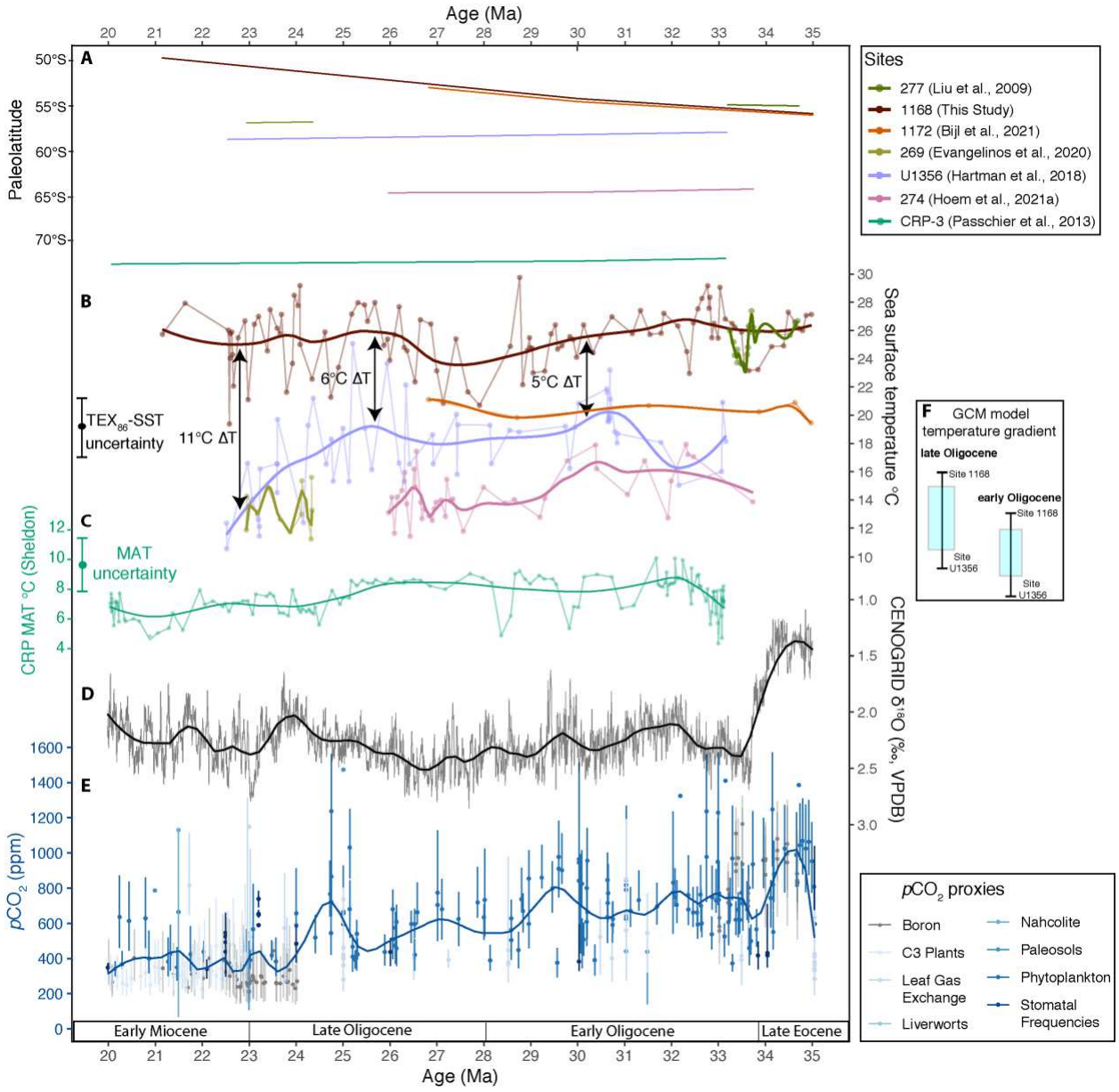

**Figure 2. Late Eocene–Early Miocene Australian-Antarctic Gulf temperature records, with their paleolatitude, compared with global benthic $\delta^{18}O$ and $pCO_2$ records and GCM models:**

A) Paleolatitude evolution of sites [51]. Colors refer to sites in Figure 1. B) $TEX_{86}$- SST reconstructions. Thick lines represent smoothed long-term trends, with a local weighted polynomial regression (LOESS; span of 0.35). For the age model of Site 1168 see Supplementary Table 2. C) Mean annual air temperature (MAT) from Site CRP-3[28]. All ages in A-C are converted to GTS2012[40]. D) Benthic foraminiferal $\delta^{18}O$, smoothed by a locally weighted function over 20 kyr (thin black curve; CENOGRID[21]). Thick black curve is the LOESS smoothed (span = 0.1). E) paleo-$CO_2$ compilation from https://www.paleo-co2.org[9]. Blue curve is the LOESS smoothed (span = 0.1). F) Shows the GCM model temperature gradient (corresponding to the scale in B) between Site 1168 and Site U1356 in the Early- and Late Oligocene.

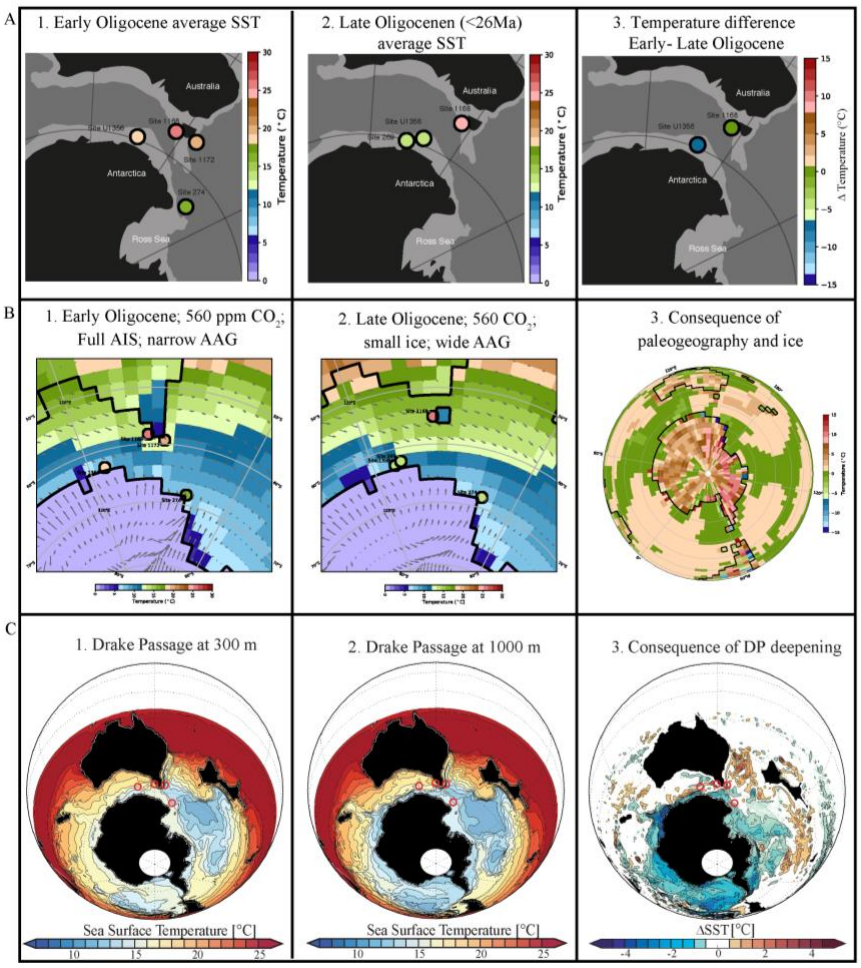


318

319 **Figure 3. Data-model experiment comparisons:**

320 A. Paleogeographic map with SST data shown in colored dots from the respective drill sites. B.

321 Fully coupled HadCM3L simulation of the Early-(33.9–28.4 Ma) and Late Oligocene (28.4–23.0

322 Ma)[23]. C. High resolution ocean model[24]. The Southern Ocean paleogeography is reconstructed

323 for Late Eocene (38 Ma), red circles indicate the studied sites.

324

325 **REFERENCES**


326 1 Hartman, J. D. *et al.* Paleoceanography and ice sheet variability offshore Wilkes Land,
327 Antarctica-Part 3: Insights from Oligocene-Miocene TEX86-based sea surface
328 temperature reconstructions. *Climate of the Past* **14**, 1275-1297,
329 doi:https://doi.org/10.5194/cp-14-1275-2018 (2018).

2 Hoem, F. S. *et al.* Temperate Oligocene surface ocean conditions offshore of Cape Adare, Ross Sea, Antarctica. *Climate of the Past* **17**, 1423-1442, doi:https://doi.org/10.5194/cp-17-1423-2021 (2021a).
3 Houben, A. J. P., Bijl, P. K., Sluijs, A., Schouten, S. & Brinkhuis, H. Late Eocene Southern Ocean Cooling and Invigoration of Circulation Preconditioned Antarctica for Full-Scale Glaciation. *Geochemistry, Geophysics, Geosystems* **20**, 2214-2234, doi:https://doi.org/10.1029/2019gc008182 (2019).
4 Liu, Z. *et al.* Global cooling during the eocene-oligocene climate transition. *Science* **323**, 1187-1190, doi:10.1126/science.1166368 (2009).
5 Bohaty, S. M., Zachos, J. C. & Delaney, M. L. Foraminiferal Mg/Ca evidence for southern ocean cooling across the eocene–oligocene transition. *Earth and Planetary Science Letters* **317**, 251-261 (2012).
6 Galeotti, S. *et al.* Antarctic Ice Sheet variability across the Eocene-Oligocene boundary climate transition. *Science* **352**, 76-80, doi:10.1126/science.aab0669 (2016).
7 Levy, R. H. *et al.* Antarctic ice-sheet sensitivity to obliquity forcing enhanced through ocean connections. *Nature Geoscience* **12**, 132-137, doi:10.1038/s41561-018-0284-4 (2019).
8 O'Brien, C. L. *et al.* The enigma of Oligocene climate and global surface temperature evolution. *Proc Natl Acad Sci U S A* **117**, 25302-25309, doi:10.1073/pnas.2003914117 (2020).
9 Hoenisch, B. *Paleo-CO2 data archive (Version 1) [Data set]. Zenodo.*, 2021).
10 Gasson, E. *et al.* Uncertainties in the modelled CO 2 threshold for Antarctic glaciation. *Climate of the Past* **10**, 451-466 (2014).
11 Goldner, A., Herold, N. & Huber, M. Antarctic glaciation caused ocean circulation changes at the Eocene–Oligocene transition. *Nature* **511**, 574-577 (2014).
12 Paxman, G. J. *et al.* Reconstructions of Antarctic topography since the Eocene–Oligocene boundary. *Palaeogeography, palaeoclimatology, palaeoecology* **535**, 109346 (2019).
13 Bijl, P. K. *et al.* Paleoceanography and ice sheet variability offshore Wilkes Land, Antarctica-Part 2: Insights from Oligocene-Miocene dinoflagellate cyst assemblages. *Climate of the Past* **14**, 1015-1033, doi:https://doi.org/10.5194/cp-14-1015-2018 (2018).
14 Sangiorgi, F. *et al.* Southern Ocean warming and Wilkes Land ice sheet retreat during the mid-Miocene. *Nature communications* **9**, 317, doi:10.1038/s41467-017-02609-7 (2018).
15 Singh, H. K., Bitz, C. M. & Frierson, D. M. The global climate response to lowering surface orography of Antarctica and the importance of atmosphere–ocean coupling. *Journal of Climate* **29**, 4137-4153 (2016).
16 Hill, D. J. *et al.* Paleogeographic controls on the onset of the Antarctic circumpolar current. *Geophysical Research Letters* **40**, 5199-5204 (2013).
17 England, M. H., Hutchinson, D. K., Santoso, A. & Sijp, W. P. Ice–atmosphere feedbacks dominate the response of the climate system to Drake Passage closure. *Journal of Climate* **30**, 5775-5790, doi:https://doi.org/10.1175/JCLI-D-15-0554.1 (2017).
18 Evangelinos, D. *et al.* Absence of a strong, deep-reaching Antarctic Circumpolar Current zonal flow across the Tasmanian gateway during the Oligocene to early Miocene. *Global and Planetary Change* **208**, 103718, doi:https://doi.org/10.1016/j.gloplacha.2021.103718 (2022).

19 Knorr, G. & Lohmann, G. Climate warming during Antarctic ice sheet expansion at the Middle Miocene transition. *Nature Geoscience* **7**, 376-381, doi:10.1038/ngeo2119 (2014).
20 Kennedy, A. T., Farnsworth, A., Lunt, D., Lear, C. H. & Markwick, P. Atmospheric and oceanic impacts of Antarctic glaciation across the Eocene–Oligocene transition. *Philosophical Transactions of the Royal Society A: Mathematical, Physical and Engineering Sciences* **373**, 20140419 (2015).
21 Westerhold, T. *et al.* An astronomically dated record of Earth's climate and its predictability over the last 66 million years. *Science* **369**, 1383-1387, doi:https://doi.org/10.1126/science.aba6853 (2020).
22 Lear, C. H., Rosenthal, Y., Coxall, H. K. & Wilson, P. Late Eocene to early Miocene ice sheet dynamics and the global carbon cycle. *Paleoceanography* **19**, doi:10.1029/2004PA001039 (2004).
23 Kennedy-Asser, A., Lunt, D. J., Farnsworth, A. & Valdes, P. Assessing mechanisms and uncertainty in modeled climatic change at the Eocene-Oligocene transition. *Paleoceanography and Paleoclimatology* **34**, 16-34 (2019).
24 Sauermilch, I. *et al.* Gateway-driven Southern Ocean cooling – The crucial role of ocean gyres. *Nature Communications* **2021**, doi:https://doi.org/10.1038/s41467-021-26658-1 (2021).
25 van de Lagemaat, S. H. *et al.* Subduction initiation in the Scotia Sea region and opening of the Drake Passage: When and why? *Earth-Science Reviews*, 103551, doi:https://doi.org/10.1016/j.earscirev.2021.103551 (2021).
26 Bijl, P. K. *et al.* Maastrichtian-Rupelian paleoclimates in the southwest Pacific–a critical evaluation of biomarker paleothermometry and dinoflagellate cyst paleoecology at Ocean Drilling Program Site 1172. *Climate of the Past Discussions*, 1-82 (2021).
27 Evangelinos, D. *et al.* Late Oligocene-Miocene proto-Antarctic Circumpolar Current dynamics off the Wilkes Land margin, East Antarctica. *Global and Planetary Change* **191**, 103221, doi:https://doi.org/10.1016/j.gloplacha.2020.103221 (2020).
28 Passchier, S. *et al.* Early Eocene to middle Miocene cooling and aridification of East Antarctica. *Geochemistry, Geophysics, Geosystems* **14**, 1399-1410 (2013).
29 Guitián, J. & Stoll, H. M. Evolution of Sea Surface Temperature in the Southern Mid-latitudes from Late Oligocene through Early Miocene. *Paleoceanography and Paleoclimatology*, e2020PA004199, doi:https://doi.org/10.1029/2020PA004199 (2021).
30 Hoem, F. S. *et al.* Late Eocene–early Miocene evolution of the southern Australian subtropical front: a marine palynological approach. *Journal of Micropalaeontology* **40**, 175-193, doi:https://doi.org/10.5194/jm-40-175-2021 (2021b).
31 Olbers, D., Borowski, D., Völker, C. & Woelff, J.-O. The dynamical balance, transport and circulation of the Antarctic Circumpolar Current. *Antarctic science* **16**, 439-470, doi:https://doi.org/10.1017/S0954102004002251 (2004).
32 Huber, M. *et al.* Eocene circulation of the Southern Ocean: Was Antarctica kept warm by subtropical waters? *Paleoceanography* **19** (2004).
33 Nicholson, U. & Stow, D. Erosion and deposition beneath the Subantarctic Front since the Early Oligocene. *Scientific reports* **9**, 1-9, doi:10.1038/s41598-019-45815-7 (2019).
34 Scher, H. D. *et al.* Onset of Antarctic Circumpolar Current 30 million years ago as Tasmanian Gateway aligned with westerlies. *Nature* **523**, 580-583 (2015).

35 Lyle, M., Gibbs, S., Moore, T. C. & Rea, D. K. Late Oligocene initiation of the Antarctic Circumpolar Current: Evidence from the South Pacific. *Geology* **35**, 691-694, doi:10.1130/g23806a.1 (2007).
36 Cramwinckel, M. J. *et al.* Synchronous tropical and polar temperature evolution in the Eocene. *Nature* **559**, 382-386 (2018).
37 Hutchinson, D. K. *et al.* The Eocene–Oligocene transition: a review of marine and terrestrial proxy data, models and model–data comparisons. *Climate of the Past* **17**, 269-315 (2021).
38 Exon, N. F., Kennett, J.P., Mal- one, M.J., et al.,. Site 1168. . *Proceedings of the Ocean Drilling Program Initial Reports, Ocean Drilling Program, College Station, TX., USA,* (2001).
39 Stickley, C. *et al.* in *Proceedings of the Ocean Drilling Program, Scientific Results.* 1-57 (Ocean Drilling Program, College Station TX).
40 Gradstein, F. M., Ogg, J. G., Schmitz, M. D. & Ogg, G. M. *The geologic time scale 2012*. (elsevier, 2012).
41 Schouten, S., Hopmans, E. C., Schefuß, E. & Damste, J. S. S. Distributional variations in marine crenarchaeotal membrane lipids: a new tool for reconstructing ancient sea water temperatures? *Earth and Planetary Science Letters* **204**, 265-274 (2002).
42 Hopmans, E. C., Schouten, S. & Damsté, J. S. S. The effect of improved chromatography on GDGT-based palaeoproxies. *Organic Geochemistry* **93**, 1-6 (2016).
43 Tierney, J. E. & Tingley, M. P. A TEX 86 surface sediment database and extended Bayesian calibration. *Scientific data* **2**, 1-10 (2015).
44 Kim, J.-H. *et al.* New indices and calibrations derived from the distribution of crenarchaeal isoprenoid tetraether lipids: Implications for past sea surface temperature reconstructions. *Geochimica et Cosmochimica Acta* **74**, 4639-4654, doi:10.1016/j.gca.2010.05.027 (2010).
45 O'Brien, C. L. *et al.* Cretaceous sea-surface temperature evolution: Constraints from TEX86 and planktonic foraminiferal oxygen isotopes. *Earth-Science Reviews* **172**, 224-247 (2017).
46 Lavelle, M. Strontium isotope stratigraphy of the CRP-1 drillhole, Ross Sea, Antarctica. *Terra Antartica* **5**, 691-696 (1998).
47 McIntosh, W. 40Ar/39Ar geochronology of volcanic clasts and pumice in CRP-1 core, Cape Roberts, Antarctica. *Terra Antartica* **5**, 683-690 (1998).
48 Florindo, F., Wilson, G. S., Roberts, A. P., Sagnotti, L. & Verosub, K. L. Magnetostratigraphic chronology of a late Eocene to early Miocene glacimarine succession from the Victoria Land Basin, Ross Sea, Antarctica. *Global and Planetary Change* **45**, 207-236 (2005).
49 Marshall, J., Adcroft, A., Hill, C., Perelman, L. & Heisey, C. A finite-volume, incompressible Navier Stokes model for studies of the ocean on parallel computers. *Journal of Geophysical Research: Oceans* **102**, 5753-5766 (1997).
50 Matthews, K. J. *et al.* Global plate boundary evolution and kinematics since the late Paleozoic. *Global and Planetary Change* **146**, 226-250 (2016).
51 van Hinsbergen, D. J. *et al.* A paleolatitude calculator for paleoclimate studies. *PloS one* **10**, e0126946, doi:10.1371/journal.pone.0126946 (2015).
52 Hutchinson, D. K. *et al.* Climate sensitivity and meridional overturning circulation in the late Eocene using GFDL CM2. 1. *Climate of the Past* **14**, 789-810 (2018).

53 Viebahn, J. P., von der Heydt, A. S., Le Bars, D. & Dijkstra, H. A. Effects of Drake Passage on a strongly eddying global ocean. *Paleoceanography* **31**, 564-581 (2016).
54 Hochmuth, K. *et al.* The evolving paleobathymetry of the circum-Antarctic Southern Ocean since 34 Ma: A key to understanding past cryosphere-ocean developments. *Geochemistry, Geophysics, Geosystems* **21**, e2020GC009122 (2020).
55 Lacasce, J. H., Escartin, J., Chassignet, E. P. & Xu, X. Jet instability over smooth, corrugated, and realistic bathymetry. *Journal of Physical Oceanography* **49**, 585-605 (2019).
56 Müller, R. D. *et al.* GPlates: building a virtual Earth through deep time. *Geochemistry, Geophysics, Geosystems* **19**, 2243-2261, doi:10.1029/2018GC007584 (2018).

## ACKNOWLEDGMENTS

This work used archived samples and data provided and curated by the IODP and its predecessors. This work was financially supported by the NWO polar programme (ALW.2016.001). We thank José Guitián, Heather Stoll and Lena Thöle for providing the subset of samples from ETH Zürich and Mariska Hoorweg for technical support. IS and PB acknowledges funding through ERC starting grant 802835 “OceaNice”. MH acknowledges support from NSF OPP grant 1842059.

## AUTHOR CONTRIBUTIONS

PKB and FS designed the research. FSH conducted the research and wrote the paper with input from all co-authors. PKB converted the age model to the GTS2012 timescale. FSH requested, processed and integrated samples for TEX86 paleothermometry. FSH, PKB, FS and FP interpreted the TEX86-SST data. IS made the high resolution the ocean model simulation. AKA and MH made the fully coupled general circulation model simulation. All co-authors approve the manuscript and agrees to its submission.

## COMPETING INTERESTS

The authors declare no competing interests.

# Supplementary Files

This is a list of supplementary files associated with this preprint. Click to download.

- TableS2GDGTs.xlsx
- Supplementaryinformationfinal.pdf